Jarzynski matrix equality: Calculating the free-energy difference by nonequilibrium simulations with an arbitrary initial distribution

Biao Wan,[1] Cheng Yang,[1] Yanting Wang,[2] and Xin Zhou[1,*]

[1]*School of Physical Sciences, University of Chinese Academy of Sciences, Beijing 100049, China*

[2]*State Key Laboratory of Theoretical Physics, Institute of Theoretical Physics, Chinese Academy of Sciences, Beijing 100190, China*

(Received 13 August 2015; published 14 April 2016)

The Jarzynski equality (JE) method, which relates the work of a nonequilibrium process to the free-energy difference between its initial and final states, provides an efficient way to calculate free energies of thermodynamic systems in simulations or experiments. However, more extensive applications of the JE are hindered by the requirement that the initial state must be in equilibrium. In this work we extend the JE method to be the Jarzynski matrix equality (JME) method, which relates the work of trajectories connecting metastable conformational regions to their local free energies, and thus we can estimate the free energy from the nonequilibrium trajectories starting from an almost arbitrary initial distribution. We then apply the JME to toy models, Lennard-Jones fluids, and polymer chain models, demonstrating its efficiency in free-energy calculations with satisfactory accuracy. The JME extends the applicability of the nonequilibrium methods to complex systems whose initial equilibrium states are difficult to reach.

DOI: 10.1103/PhysRevE.93.043312

I. INTRODUCTION

Over the past two decades, important progress in nonequilibrium statistical physics has led to the development of fluctuation theorems [1–3] and, in particular, the Jarzynski equality (JE) [4,5], which relates the distribution of irreversible works of a nonequilibrium process to the free-energy difference between initial and final states. The JE can be written as

$$\exp(-\beta\triangle A) = \langle \exp(-\beta W)\rangle, \tag{1}$$

where $\beta = \frac{1}{k_B T}$ is the reciprocal of temperature multiplied by the Boltzmann constant k_B, $\triangle A$ is the free-energy difference between the initial and final states, and $\langle\cdots\rangle$ denotes the average over the ensemble of trajectories that starts from the equilibrium distribution of the initial state and ends with the final state. The work W is defined as

$$W[x(t)] = \int_0^\tau \frac{\partial H(x(t),\Lambda(t))}{\partial \Lambda}\dot{\Lambda}\, dt, \tag{2}$$

where $x(t)$ is a simple notation of a trajectory in the conformational space within the time interval $[0,\tau]$. The trajectory can be generated by a deterministic or a stochastic dynamic under the time-dependent Hamiltonian $H(x,\Lambda(t))$ with the protocol $\Lambda(t)$. Here $\dot{\Lambda}$ denotes the time derivative of $\Lambda(t)$. Thus the work is a functional of the nonequilibrium trajectory $x(t)$. In this paper $x(t)$ represents the whole trajectory and a particular conformation of the trajectory at time t is denoted by x_t.

The JE method provides a direct way to estimate the free-energy difference in experiments, such as single-molecule pulling [6–8], as well as to calculate the free energy by nonequilibrium molecular dynamics (MD) simulations [9–12]. However, there is a major difficulty in applying the JE. The right-hand side of Eq. (1), the ensemble average of an exponential function of work, is dominated by rare trajectories with small work values. Therefore, inadequate sampling of these rare events results in a biased estimation, as described by the Jensen inequality [5]. One way to overcome this problem, as done in single-molecule pulling experiments, is to apply a very stiff spring potential to obtain a work distribution with an approximate Gaussian shape [13], so the ensemble average of the exponential function of work can be estimated with satisfactory accuracy from a relatively small number of trajectories [14–17]. In more general cases, however, the work distribution may deviate far from Gaussian, so the Gaussian approximation cannot estimate free energy very well. Another way is to use enhanced sampling techniques to generate more small-work trajectories [18–21], which enhances simulation efficiency several times.

Another essential difficulty in applying the JE is to achieve a well-equilibrated state as the starting point of nonequilibrium trajectories, which may require a very (even impractically) long simulation time for a complex system, e.g., macroscopic biomolecules, to reach its equilibrium, since the conformational space consists of multiple long-lifetime metastable states separated by high free-energy barriers. Some recent attempts tried to extend the applicability of the JE by eliminating the requirement that the initial state must be well equilibrated. For instance, Maragakis *et al.* [22] extended the Crooks theorem [2] to calculate the free-energy difference between two metastable conformational regions. Similarly, Junier *et al.* [23] derived a fluctuation relation under partial-equilibrium conditions to estimate the free-energy branches of metastable states in single-molecule experiments. Very recently, a theoretical extension of the JE with an arbitrary initial distribution was also discussed by Gong and Quan [24]. However, these works have to apply the time-reverse process of nonequilibrium trajectories to compensate for the deviation of the initial distribution from the equilibrium one.

In this paper we extend the JE to be compatible with an (almost) arbitrary initial distribution and any nonequilibrium protocol without performing the time-reversal process by presenting a transformation matrix form of the extended JE, named the Jarzynski matrix equality (JME), which is built on the free energies of the initial and final metastable substates of

*Author to whom correspondence should be addressed: xzhou@ucas.ac.cn

a nonequilibrium process. The initial distribution is in a local equilibrium inside each metastable conformational region (potential basin or superbasin) but is not equilibrated among these regions, which is very easy to reach from any initial distribution after a short-time local equilibrium relaxation. In other words, the whole conformational space is composed of some metastable regions (substates) and the local equilibrium inside each region is quickly achieved. Since transitions from one region to another have to overcome free-energy barriers, reaching the equilibrium among those regions requires a great deal of time. Therefore, in our method, an arbitrary initial distribution can easily reach local equilibrium distributions inside metastable substates after a short-time relaxation, but the long-time relaxation towards the equilibrium among metastable substates is avoided [25,26]. Consequently, the JE connecting the free energy of well-equilibrated initial and final states is now replaced by the JME connecting the free energies of the metastable substates in the initial and final states.

The essential idea of the JME is formulated as follows. We suppose that the whole conformational space is divided into some nonoverlapping conformational regions (metastable substates); then the total partition function of a system $Z = \int e^{-\beta H(x)} dx$ is the summation of the local partition functions of these substates $Z = \sum_\mu Z_\mu$, where $Z_\mu = \int_{\Gamma_\mu} e^{-\beta H(x)} dx$. Here the integral is confined in the conformational region Γ_μ of the substate μ, which may be a potential energy basin or many connected basins in the original conformational space or a free-energy basin in a coarse-grained space. The local equilibrium inside each of those metastable substates can usually be quickly reached [27] and only transitions between them require a very long time to happen. When a nonequilibrium process is applied, we have $Z_\mu(f) = \sum_\nu \pi_{\mu\nu}(f,i) Z_\nu(i)$, where i and f denote the initial and final states of the nonequilibrium process, respectively. The transition matrix $\pi_{\mu,\nu}(f,i) = T_{\mu\nu}(f,i)\langle \exp(-\beta W)\rangle_{\mu\nu}$, where $T_{\mu\nu}(f,i)$ is the transition probability of trajectories starting from substate ν of the initial state i to the substate μ of the final state f and $\langle\cdot\rangle_{\mu\nu}$ is the ensemble average over all the transition trajectories from $\nu(i)$ to $\mu(f)$. In particular, if the final state is chosen to be identical to the initial one, the above relation is reduced to the linear equation $Z_\mu = \sum_\nu \pi_{\mu\nu} Z_\nu$, which can be used to solve Z_μ and thus the free energy of the whole system.

II. THEORY AND METHODS

A. Basic theory

For an arbitrary initial distribution $\rho_{\rm init}(x_0)$, we can reproduce the equilibrium distribution of the initial Hamiltonian $H(x;\lambda_0)$, $\rho_{eq,0}(x_0)$, by defining the weight function $\omega(x_0) = \frac{\rho_{eq,0}(x_0)}{\rho_{\rm init}(x_0)}$; then we have

$$\langle \omega(x_0)\delta(x - x_\tau)\exp\{-\beta W[x(t)]\}\rangle = \frac{\exp[-\beta H(x;f)]}{Z(i)}, \tag{3}$$

where $\langle\cdots\rangle$ is the ensemble average over trajectories starting from the initial distribution $\rho_{\rm init}(x_0)$ and $H(x;f)$ is the final Hamiltonian. Equation (3) is a direct extension of the JE with an arbitrary initial distribution. It is also an extension of the formula given by Hummer and Szabo [6]. The original JE can be obtained by integrating both sides of Eq. (3) with respect to x after setting $\omega(x_0) = 1$. The reweighting itself is not helpful, since $\omega(x_0)$ is usually an exponential function with a very wide range of values except in very low (one or two) dimensions [26], but it facilitates our local equilibrium approximations described below.

B. Local equilibrium approximation

As mentioned before, we can usually divide the conformational space of a system into many regions and the local equilibrium inside each of the regions can be achieved in a short-time simulation, while the equilibration between regions needs a much longer time. Therefore, after a short relaxation simulation, an arbitrary initial distribution can relax to a locally equilibrated distribution in proportion to the equilibrium distribution inside each of the conformational regions (metastable substates) $\rho(x;0^+) = \sum_\mu c_\mu \rho_{eq}(x)\Theta_\mu(x)$. Here $\rho(x;0^+)$ is the short-time relaxed distribution and we can reset it as $P_{\rm init}(x)$ at $t = 0$. In addition, c_μ is a constant depending on the index of substate μ and $\Theta_\mu(x)$ is the characteristic function of substate μ, which is unity if the conformation x is inside substate μ and otherwise zero. Note that the way to divide the conformational space into metastable substates depends on the relaxation time: If the relaxation time is very short, we may have to divide the conformational space into many small substates to guarantee that the local distribution inside each of the substates is in equilibrium after the relaxation. A simpler division with fewer and larger substates can be achieved by a longer relaxation simulation, which allows some adjacent small substates to merge together and form more stable substates. Therefore, without losing generality, we assume that the weighting function $\omega(x_0)$ in Eq. (3) is approximately a constant ω_ν for all x_0 inside the substate ν, but the value of ω_ν varies with respect to the index of substate ν [26]. This approximation greatly simplifies Eq. (3) in practice.

We now have

$$\sum_\nu \left\langle \omega_\nu \Theta^i_\nu(x_0)\delta(x - x_\tau)\exp\{-\beta W[x(t)]\}\right\rangle = \frac{\exp[-\beta H(x;f)]}{Z(i)}, \tag{4}$$

where the indices i and f represent the initial and final Hamiltonians, respectively. By multiplying the characteristic function of the final state $\Theta^f_\mu(x)$ on both sides of Eq. (4) and integrating both sides with respect to x, we have

$$\int dx \sum_\nu \Theta^f_\mu(x)\omega_\nu \left\langle \Theta^i_\alpha(x_0)\delta(x - x_\tau)\exp\{-\beta W[x(t)]\}\right\rangle = \frac{Z(f)}{Z(i)}\int dx\, \Theta^f_\mu(x)\rho_{eq,f}(x). \tag{5}$$

Here $\rho_{eq,f}(x)$ is the equilibrium probability function of the final state, which is equal to $\frac{1}{Z(f)}\exp[-\beta H(x;f)]$. We rewrite the local partition function of the metastable substate $Z_\nu = \int \Theta_\nu(x) e^{-\beta H(x)} dx$ and $p_\nu \propto Z_\nu$, where p_ν is the equilibrium probability of visiting substate ν. Eventually, we obtain the

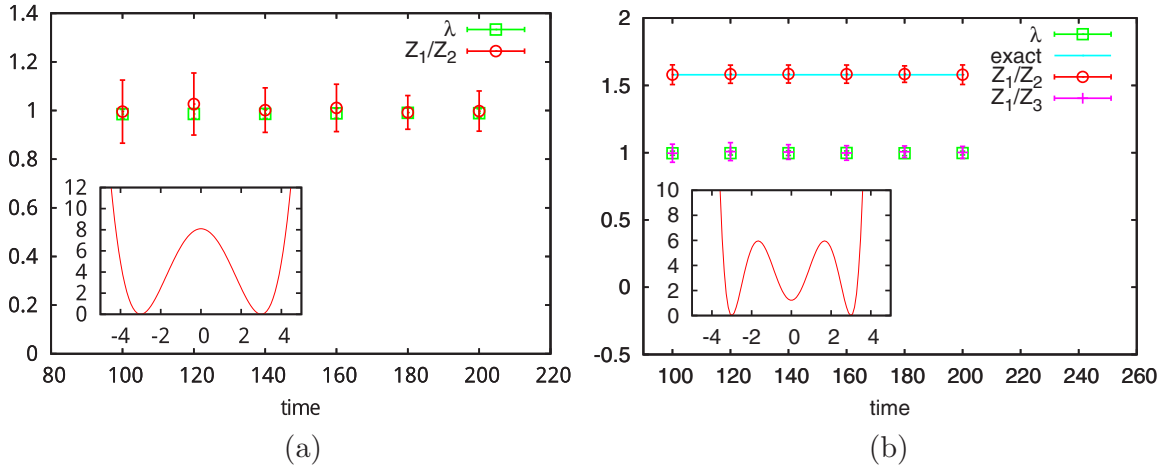

FIG. 1. Nonequilibrium simulation results of the one-dimensional symmetric multiple wells. (a) Simulation results for the double-well potential. The X axis is the simulation duration of a single trajectory. The green symbols denote the eigenvalues of the transition matrix and the red ones denote the partition function ratios of state 1 over state 2. The inset depicts the potential landscape. (b) Simulation results for the triple-well potential. The green symbols denote the eigenvalues of the matrix, the red ones denote the partition function ratios of state 1 over state 2, and the magenta ones denote the ratios of state 1 over state 3. The inset depicts the corresponding potential.

main expression of the JME

$$\sum_{\nu} \pi_{\mu\nu}(f,i) Z_{\nu}(i) = Z_{\mu}(f), \tag{6}$$

where $\pi_{\mu\nu}(f,i) = \frac{n_{\mu\nu}}{n_{\nu}(0)} \frac{1}{n_{\mu\nu}} \sum_k \exp(-\beta W_k) = T_{\mu\nu}(f,i) \frac{1}{n_{\mu\nu}} \sum_k \exp(-\beta W_k)$. Here $n_{\nu}(0)$ is the total number of trajectories starting from substate ν in the initial state and $n_{\mu\nu}$ is the number of trajectories starting from ν and ending in substate μ in the final state. The summation of k is limited to the transition trajectories from ν to μ and W_k is the work along the transition trajectory k. In addition, $T_{\mu\nu}(f,i) = \frac{n_{\mu\nu}}{n_{\nu}(0)}$ is the transition probability of nonequilibrium trajectories starting from state $\nu(i)$ and ending in state $\mu(f)$. For equilibrium processes $W_k = 0$, Eq. (6) becomes the normal detailed balance condition.

C. Loop protocol and linear equation

If we choose a loop nonequilibrium protocol where the initial Hamiltonian is identical to the final one, i.e., $\Lambda(t_0) = \Lambda(\tau)$, Eq. (6) becomes a linear equation $\sum_{\nu} \pi_{\mu\nu} Z_{\nu} = Z_{\mu}$ or

$$\Pi \mathbf{Z} = \mathbf{Z}, \tag{7}$$

which offers a practical way to estimate the local partition functions $\{Z_{\mu}\}$. Here $\mathbf{Z} = (Z_1, \ldots, Z_{\mu}, \ldots, Z_n)^T$. Since the matrix elements are non-negative, Π is a positive and nonreductive matrix. According to the Perron-Frobenius theorem, a positive and nonreductive matrix has only one eigenvector whose components all have the same sign, corresponding to the eigenvalue with the largest modulus. Therefore, Π has a unique non-negative vector $\mathbf{Z}$ corresponding to the eigenvalue $\lambda = 1$ in Eq. (7). In principle, the corresponding eigenvalue should be unity. In practice, however, due to numerical and statistical errors, it might slightly differ from unity. The deviation of the eigenvalue from unity is a good criterion for determining whether the number of generated nonequilibrium trajectories is sufficient.

III. RESULTS AND ANALYSIS

To check its validity, we applied the JME to three kinds of systems: one-dimensional multiple-well potentials, Lennard-Jones fluids around the liquid-solid coexistence region, and a polymer chain with closing and opening end-end states. The implementation of the JME contains four steps: (i) Randomly choose many initial conformations (with a significant number of conformations in each important metastable substate) and then relax them shortly under the initial Hamiltonian to serve as the initial conformations at $t = 0$ with the relaxation time so chosen that each state can reach the local equilibrium; (ii) start the nonequilibrium simulations with the loop protocol $\Lambda(0) = \Lambda(\tau)$ from the prepared initial conformations; and (iii) calculate the matrix elements of Π and its unique same-sign eigenvector and the corresponding eigenvalue λ. The eigenvector gives $\mathbf{Z}$ with an arbitrary constant coefficient and whether λ approximately equals 1 provides a criterion for evaluating the validity of the calculation.

A. One-dimensional toy models

We first consider a simple one-dimensional symmetric double-well potential, shown in Fig. 1(a),

$$U = \tfrac{1}{2} k (q^2 - 9)^2. \tag{8}$$

A particle moving in this potential is simulated according to the overdamped Langevin dynamics with $\beta = 1$. The mobility of the particle is 0.2. A nonequilibrium loop protocol linearly changes the parameter k as a function of time from $k(0) = 0.2$ to $k(\tau) = 0.2$, namely, $k(t) = 0.2 - 0.36t/\tau$ when $0 < t \leqslant \frac{\tau}{2}$ and $k(t) = 0.02 + 0.36t/\tau$ when $\frac{\tau}{2} < t \leqslant \tau$.

We ran six sets of nonequilibrium simulations with different simulation durations of $\tau = 100$, 120, 140, 160, 180, and 200, respectively. For each set, we generated a total 2000 trajectories and the initial allocation of these trajectories in the two states was that the left potential well had 1200 trajectories and the right well had 800 trajectories. Each trajectory initially

went through a short equilibration simulation to reach the local equilibrium distribution inside its initial potential well. The results are shown in Fig. 1(a). The green symbols denote the eigenvalues of the transition matrix Π and the red ones denote the partition function ratios of state 1 over state 2, whose theoretical values should both be 1. As expected, the values of the two parameters calculated from different simulation durations are all close to 1. The error bars in the figure are the standard deviations obtained by repeating the simulations and calculations 100 times.

We also applied the method to the overdamped motion of a particle in a one-dimensional triple-well potential

$$U = \tfrac{1}{2}k(q^2-9)^2(q^2+0.3), \tag{9}$$

where we set $k = 0.1$ and $\beta = 1$. The mobility of the particle is 0.2. The three states are labeled 1, 2, and 3 from left to right, as shown in Fig. 1(b). The exact partition function values are $Z_1 = 1.58Z_2$ and $Z_1 = Z_3$. The nonequilibrium protocol is similar to the previous example. We ran six sets of nonequilibrium simulations with different durations of $\tau = 100$, 120, 140, 160, 180, and 200, respectively. For each set, we generated 3000 trajectories evenly distributed in the three states to estimate the matrix elements. The results are shown in Fig. 1(b). The green symbols denote the eigenvalues of the transition matrix, whose ideal value should be 1; the red symbols denote the partition function ratios of state 1 over state 2, whose ideal value should be 1.58; and the magenta symbols denote the ratios of state 1 over state 3, whose ideal value should be unity. The values calculated from the trajectories with different simulation lengths are all close to their ideal values. The error bars in the figure are the standard deviations obtained by repeating the simulations and calculation 100 times.

B. Lennard-Jones liquid-solid coexistence

Next we applied the JME to a 32-particle Lennard-Jones (LJ) system inside a cubic box with a side length of 11.8 Å and the periodic boundary condition applied. The system was coupled to a Nóse-Hoover thermostat with temperature $T =$ 55 K, at which the liquid and solid states have similar free energies. The pairwise LJ interaction

$$u(r) = 4\epsilon\left(\frac{\sigma^{12}}{r^{12}} - \frac{\sigma^6}{r^6}\right), \tag{10}$$

where the cutoff radius was 5.8 Å smaller than half of the simulation box length. At evenly distributed 40 time points during the whole nonequilibrium simulation period, we uniformly changed the parameter ϵ from 0.34 to 0.35, then from 0.35 to 0.33, and finally from 0.33 to 0.34. The unit of ϵ was kcal/mol. The nonequilibrium work was calculated based on Eq. (2). The fractions of the liquid and solid states can be calculated from the nonequilibrium simulations based on Eq. (6). To distinguish the liquid and solid states, we employed the local bond order parameters measuring the local structure around a particle [28], defined as

$$q_{lm}(i) = \frac{1}{N_b(i)}\sum_{j=1}^{N_b(i)} Y_{lm}(\tilde{r}_{ij}), \tag{11}$$

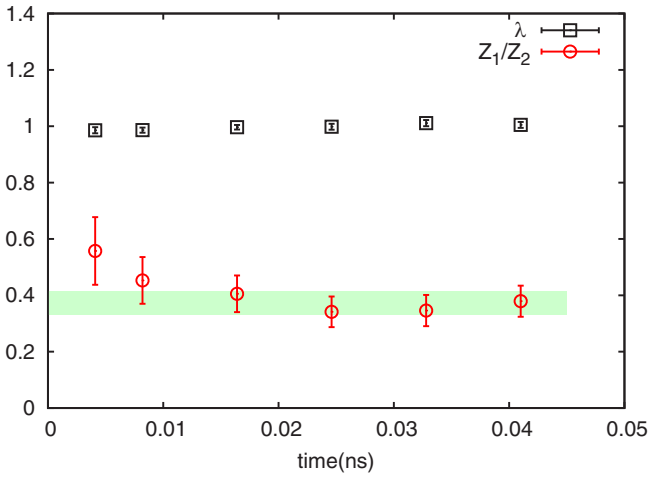

FIG. 2. Nonequilibrium simulation results of the LJ system. The X axis is the simulation duration of a single trajectory. The black symbols denote the eigenvalues of the matrix and the red ones denote the partition function ratios of the solid state over the liquid state. As a reference, the mean value from 20 sets of 400 1-ns equilibrium simulations (green shadow) is 0.37.

where $\tilde{r}_{ij}$ is the unit vector from particle i to particle j, the summation goes over all neighboring particles $N_b(i)$ of particle i, and $Y_{lm}(\tilde{r}_{ij})$ is the spherical harmonic function, with l and m taking integer values of $l = 0,1,\ldots,$ and $m = -l,\ldots,l$. Specifically, q_6 is known as a good order parameter for distinguishing the liquid and solid phases [28]. In simple liquids, there are no preferred orientations around a particle and thus the structural correlation decays rapidly. In contrast, for particles in a solidlike environment the vectors are correlated:

$$\mathbf{q}_6(i)\cdot\mathbf{q}_6(j) = \sum_{m=-6}^{6} q_{6m}(i)\cdot q_{6m}^*(j), \tag{12}$$

where the asterisk indicates the complex conjugate. The average of the correlation functions provides a rough criterion for distinguishing the liquid phase and the solid phase as [29]

$$s = \frac{1}{32}\sum_i \sum_{j=1}^{N_b(i)} \frac{\mathbf{q}_6(i)\cdot\mathbf{q}_6(j)}{|q_6(i)||q_6(j)|}. \tag{13}$$

In our MD simulations of this system, the value of the parameter changes continuously from 0 to 12 when it evolves from the liquid phase to the solid phase. We consider the system to be in the liquid phase when $s < 7$ and solid otherwise.

Figure 2 shows six sets of nonequilibrium simulations with the simulation length of the individual trajectory τ ranging from 4.8 to 42 ps. For each set of simulations, we generated 200 trajectories starting from liquid and the other 200 from solid. The bootstrap method [30] was used to estimate errors. Each trajectory first went through a 0.2-ps equilibration simulation for initial local relaxation. The positive eigenvalues of the transition matrices approximately equal 1 due to the small work fluctuations in our simulations. For comparison, we also simulated 20×400 equilibrium simulation trajectories with $\tau = 1$ ns for each and then counted the numbers of trajectories in the liquid and solid states as a function of time

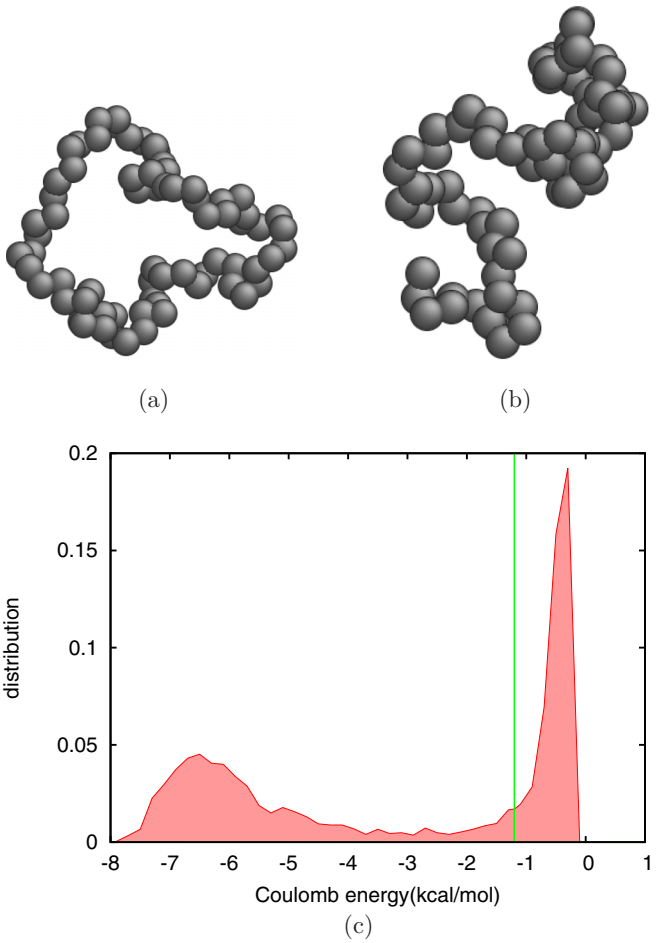

FIG. 3. (a) End-end closing configuration and (b) end-end opening configuration of the polymer chain system. (c) Coulomb energy distribution from 5000 samples showing two well-separated peaks: the energy greater than -1.2 belongs to the end-end opening state and the energy less than -1.2 belongs to the end-end closing configuration.

$t \in [0,\tau]$, $N_1(t)$ and $N_2(t)$. We have found that the ratio of the probabilities visiting the two states $C(t) = N_1(t)/N_2(t)$ vibrationally approaches a constant value when $t > 0.5$ ns. The constant value is regarded as a reference for the ratio of equilibrium visiting probabilities in the two states and its error bar is the standard deviation calculated by dividing these trajectories into 20 different groups. The ratio of the solid-state partition function to the liquid-state one obtained from 15-ps trajectories is already in good agreement with the reference value.

C. Opening and closing polymer chain

Finally we studied a model polymer chain consisting of 70 atoms. The atoms interact with each other by the pairwise LJ potential and the neighboring atoms along the chain are connected by a harmonic spring potential. In addition, we applied the Coulomb interaction to the two ending atoms of the chain to adjust the ratio of two metastable states, namely, the end-end closing and opening states, shown in Figs. 3(a) and 3(b), respectively. The distribution of the Coulomb energy

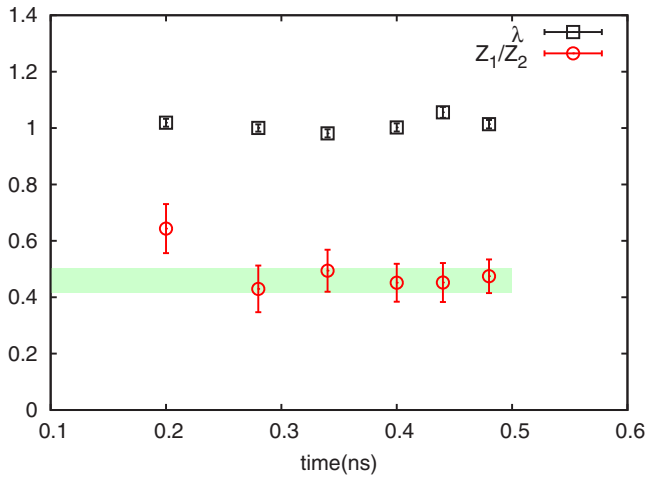

FIG. 4. Nonequilibrium simulation results for the polymer chain model. The black symbols denote the eigenvalues of the matrix and the red ones denote the partition function ratios of the open state over the loop state. As a reference, the mean value of 20 sets of 500 2.5-ns equilibrium simulations (green shadow) is 0.45.

shown in Fig. 3(c) has two well-separated peaks, which allows it to serve as an order parameter to distinguish the open and close states. The Coulomb potential is

$$U_e(r) = -\frac{\alpha}{r}, \tag{14}$$

where $\alpha = \frac{Q_1 Q_2}{4\pi\epsilon}$, with Q_1 and Q_2 being the charges of the two ending atoms and ϵ the dielectric constant. Here an isolated system without any periodic images is considered and the cutoff radius of the Coulomb interaction is 50 Å. Since the Coulomb interaction controls the opening-closing transition, the simplest way of enhancing the transition is to manipulate the coefficient α.

The nonequilibrium simulation was evenly divided into 20 time segments and the parameter α was uniformly changed stepwise from 1/34 to 1/40 at the starting time point of the first 10 segments and then uniformly increases stepwise back to 1/34 at the starting time point of the second 10 simulation segments. The nonequilibrium work is then $W = \sum_i \delta U_e^i$, where $\delta U_e^i = -\frac{\delta\alpha_i}{r_i}$ is the Coulomb energy change at the ith α variation, with r_i the end-end distance. Figure 4 shows six sets of nonequilibrium simulations with the length of each trajectory ranging from $\tau = 0.2$ to 0.48 ns. The system temperature was fixed at $T = 300$ K by coupling to a Langevin thermostat. For each set of simulations, 500 trajectories were generated and each state initially had 250 trajectories, thus the total simulation time in each protocol is $t_{\text{total}} = 500\tau$. At the beginning, each trajectory went through a 2-ps simulation to reach the local equilibrium inside each state. For comparison, we also simulated 20×500 equilibrium simulation trajectories with $\tau = 2.5$ ns for each and then counted the numbers of trajectories in the two states as a function of time $t \in [0,\tau]$, $N_1(t)$ and $N_2(t)$. The ratio of the visiting probabilities in the two states $C(t) = N_1(t)/N_2(t)$ was found to vibrationally approach a constant value when $t > 1$ ns. The constant value is regarded as a reference for the ratio of equilibrium visiting probabilities in the two states

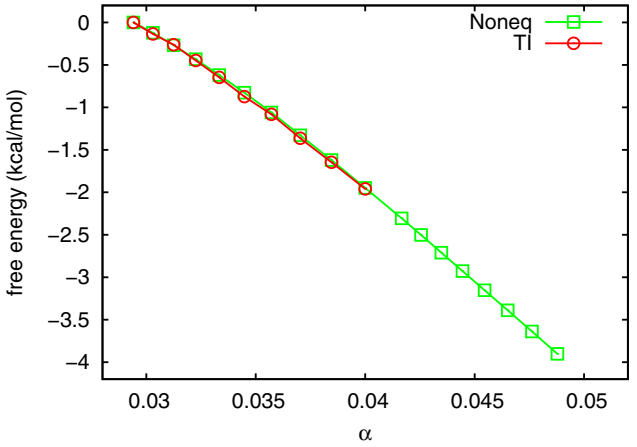

FIG. 5. Free-energy difference as a function of the Coulomb interaction strength α changing from $1/34$ to $1/20$. The green line is the free energy as a function of α from the nonequilibrium simulation using Eq. (6) with an initial ratio of 0.43. As a reference, the red one is the free energy as a function of α in [1/34,1/25] calculated by the thermodynamic integration method.

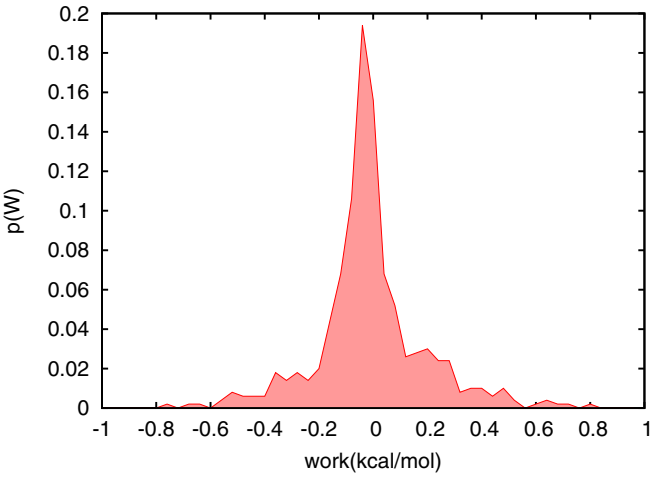

FIG. 6. Work distribution of the fastest nonequilibrium simulation for the polymer chain model.

and its error bar is the standard deviation calculated by dividing these trajectories into 20 different groups. As shown in Fig. 4, the nonequilibrium simulations with $\tau > 0.28$ ns are in agreement with the equilibrium simulation result.

After obtaining the initial $Z_\nu(i)$, it is straightforward to estimate the free energy of any final state based on Eq. (6). In the polymer chain system, 250 170-ps nonequilibrium trajectories with the protocol evenly and stepwise change α from $1/34$ to $1/20$ at 17 time points, so the total simulation time of all trajectories is 42.5 ns. In Fig. 5 the green line denotes the calculated free energy as a function of α. For comparison, we also calculated the free energy with α in [1/34,1/25] by the thermodynamic integration (TI) method based on equilibrium simulations [31]. We can see that the free-energy profile obtained from the nonequilibrium simulation is in good agreement with the value obtained by the TI method.

IV. CONCLUSION AND DISCUSSION

The major advantage of the JME over the JE is not to require the global equilibrium initial distribution, so the JME can be applied to complex systems whose initial equilibrium distribution is usually hard to obtain. In addition, in the JME, trajectories are clustered into different groups according to their beginning and ending metastable substates and the exponential average of work is estimated separately in each group. Since the work fluctuation inside each group should not be larger than that of all trajectories, the grouping average may be advantageous in estimating the exponential average of work.

The key of the JME method is to choose a nonequilibrium process that can enhance the transition efficiency among metastable substates and at the same time limit the work fluctuation in each group of the nonequilibrium trajectories within the order of k_BT. For these two purposes, the applied time-dependent biased potential in the JME should be so designed that it can lower the free-energy barriers separating important metastable substates to be on the order of a few k_BT. Although this kind of biased potential was previously implemented in equilibrium simulations [31–33], we managed to adopt it in nonequilibrium simulations of the JME by applying the bias potential slowly to remove the associated nonequilibrium effects. It is essential to design the range-limited biased potential in such a way that it is mainly allocated in the transition regions between metastable substates, which usually requires some *a priori* understanding of the metastable substates, order parameters, or reaction coordinates. For example, in the polymer chain model we have studied, all the chosen nonequilibrium protocols produce small work fluctuations and enhance transitions. The work fluctuation even in the fastest nonequilibrium simulation ($\tau = 0.2$ ns), as shown in Fig. 6, is still on the order of $1k_BT$, which guarantees the accuracy of free-energy calculations.

The systems studied in this paper all have metastable substates that are known and easy to distinguish, so we can focus on the transition-related regions and design a suitable biased potential to adjust the potential energy surface in those regions. In more general cases, when the metastable substates of the system are unknown, we may have to combine the JME with one of our previously developed techniques, the reweighting ensemble dynamics method [26], to obtain a more general formula for the JME without explicitly identifying metastable substates and the transitions among them [34].

ACKNOWLEDGMENTS

Funding by the NSFC under Grants No. 11347614 and No. 11121403 and the Open Project from State Key Laboratory of Theoretical Physics is gratefully acknowledged. X.Z. thanks the Hundred Talent Program of the Chinese Academy of Sciences for financial support and D. P. Landau for discussion.

[1] G. E. Crooks, J. Stat. Phys **90**, 1481 (1998).
[2] G. E. Crooks, Phys. Rev. E **61**, 2361 (2000).
[3] R. Klages, W. Just, and C. Jarzynski, *Nonequilibrium Statistical Physics of Small Systems* (Wiley-VCH, Weinheim, 2013).
[4] C. Jarzynski, Phys. Rev. Lett. **78**, 2690 (1997).
[5] C. Jarzynski, Phys. Rev. E **56**, 5018 (1997).
[6] G. Hummer and A. Szabo, Proc. Natl. Acad. Sci. USA **98**, 3658 (2001).
[7] J. Liphardt, S. Dumont, S. B. Simth, T. Tinoco, and C. Bustamante, Science **296**, 1832 (2002).
[8] N. C. Harris, Y. Song, and C.-H Kiang, Phys. Rev. Lett. **99**, 068101 (2007).
[9] C. Jarzynski, Eur. Phys. J. B **64**, 331 (2008).
[10] G. Hummer and A. Szabo, Acc. Chem. Res. **38**, 504 (2005).
[11] S. Park, F. Ritort, E. Tajkhorshid, and K. Schutlen, J. Chem. Phys. **119**, 3559 (2003).
[12] M. O. Jensen, S. Park, E. Tajkhorshid, and K. Schutlen, Proc. Natl. Acad. Sci. USA **99**, 6731 (2002).
[13] S. Park and K. Schutlen, J. Chem. Phys. **120**, 5946 (2004).
[14] G. Hummer, J. Chem. Phys. **114**, 7330 (2001).
[15] D. M. Zuckerman and T. B. Woolf, Phys. Rev. Lett. **89**, 180602 (2002).
[16] D. M. Zuckerman and T. B. Woolf, Chem. Phys. Lett. **351**, 445 (2002).
[17] J. Gore, F. Ritort, and C. Bustamante, Proc. Natl. Acad. Sci. USA **100**, 12564 (2003).
[18] C. Jarzynski, Proc. Natl. Acad. Sci. USA **98**, 3636 (2001).
[19] S. X. Sun, J. Chem. Phys. **118**, 5769 (2003).
[20] F. M. Ytreberg and D. M. Zuckerman, J. Chem. Phys. **120**, 10876 (2004).
[21] R. Chelli, C. Gellini, G. Pietraperzia, E. Giovannelli, and C. Cardini, J. Chem. Phys. **138**, 214109 (2013).
[22] P. Maragakis, M. Spichty, and M. Karplus, Phys. Chem. B **112**, 6168 (2008).
[23] I. Junier, A. Mossa, M. Manosas, and F. Ritort, Phys. Rev. Lett. **102**, 070602 (2009).
[24] Z. Gong and H. T. Quan, Phys. Rev. E **92**, 012131 (2015).
[25] X. Huang, G. R. Bowman, S. Bacallado, and V. S. Pande, Proc. Natl. Acad. Sci. USA **106**, 19765 (2009).
[26] L. C. Gong and X. Zhou, Phys. Rev. E **80**, 026707 (2009).
[27] M. A. Miller and D. J. Wales, J. Chem. Phys. **111**, 6610 (1999).
[28] S. Auer and D. Frenkel, J. Chem. Phys. **120**, 3015 (2004).
[29] J. Russo and H. Tanaka, Sci. Rep. **2**, 505 (2012).
[30] B. Efron and R. J. Tibshirani, *An Introduction to the Bootstrap* (Chapman & Hall, New York, 1993).
[31] D. Frenkel and B. Smit, *Understanding Molecular Simulation: From Algorithms to Applications* (Academic, New York, 2001).
[32] D Chandler, J. Chem. Phys. **68**, 2959 (1978).
[33] M. J. Ruiz-Montero, D. Frenkel, and J. J. Brey, Mol. Phys. **90**, 925 (1997).
[34] C. Yang, B. Wan, S. Xu, Y. T. Wang, and X. Zhou, Phys. Rev. E **93**, 033309 (2016).